



Universidad Autónoma
de Madrid

Biblos-e Archivo
Repositorio Institucional UAM

Repositorio Institucional de la Universidad Autónoma de Madrid

<https://repositorio.uam.es>

Esta es la **versión de autor** del artículo publicado en:

This is an **author produced version** of a paper published in:

Microporous and Mesoporous Materials 310 (2021): 110634

DOI: <https://doi.org/10.1016/j.micromeso.2020.110634>

Copyright: © 2020 Elsevier Inc. This manuscript version is made available under the CC-BY-NC-ND 4.0 licence <http://creativecommons.org/licenses/by-nc-nd/4.0/>

El acceso a la versión del editor puede requerir la suscripción del recurso

Access to the published version may require subscription

[Click here to view linked References](#)

Nanoporous silicon microparticles embedded into oxidized hyaluronic acid/adipic acid dihydrazide hydrogel for enhanced controlled drug delivery

Carla Giometti França¹, Tanya Plaza², Nelson Naveas^{3,4}, Maria Helena Andrade Santana¹, Miguel Manso-Silván³, Gonzalo Recio⁵, Jacobo Hernandez-Montelongo^{2,6*}

¹Department of Materials and Bioprocess Engineering, Faculty of Chemical Engineering, Universidade Estadual de Campinas, 13083-852, Campinas, Brazil.

²Bioproducts and Advanced Materials Research Center (BioMA), Faculty of Engineering, Universidad Católica de Temuco, 4813302, Temuco Chile.

³Department of Applied Physics, Faculty of Sciences, Universidad Autónoma de Madrid, 28049, Madrid, Spain.

⁴Department of Chemical Engineering and Mining Process, Faculty of Engineering, Universidad de Antofagasta, 1270300, Antofagasta, Chile.

⁵Faculty of Engineering and Technology, Universidad de San Sebastián, 4080871, Concepcion, Chile.

⁶Department of Mathematical and Physical Sciences, Faculty of Engineering, Universidad Católica de Temuco, 4813302, Temuco, Chile.

*To whom correspondence should be addressed:

jacobo.hernandez@uct.cl

Abstract

Oxidized hyaluronic acid cross-linked with adipic acid dihydrazide (oxi-HA/ADH) forms an injectable and biocompatible hydrogel suitable for treatment of musculoskeletal diseases and for drug delivery applications. In that sense, nanoporous silicon (nPSi) can be combined with biopolymers, such as oxi-HA/ADH hydrogel, to display new characteristics, which are not exhibited by the individual constituents alone. Under this context, in this work nPSi microparticles at concentrations from 0.1% to 1% *m/v* were embedded into oxi-HA/ADH hydrogel to improve its mechanical stability and enhance its control over drug release kinetics using Rose Bengal (RB) as a model drug because its cytotoxic effect in different cancer cell lines and tumors has been previously reported. Our results showed, for both compressive force and stress strength tests, that oxi-HA/ADH hydrogel with 1% nPSi microparticles doubled the values of control samples. Moreover, samples of oxi-HA/ADH with nPSi microparticles improved RB release kinetics control over pure oxi-HA/ADH hydrogel. Finally, the cell viability of nPSi microparticles embedded into oxi-HA/ADH hydrogel was confirmed using fibroblasts.

Keywords: nanoporous silicon; oxidized hyaluronic acid; adipic acid dihydrazide; hydrogel; mechanical resistance; drug delivery

1. Introduction

Hyaluronic acid (HA) is a natural polysaccharide, which is composed of N-acetyl-D-glucosamine and D-glucuronic acid linked by β -1,4-glycosidic bonds that is biodegradable, biocompatible and non-immunogenic [1,2]. HA is prevalently distributed around cells, where it forms a pericellular film, and in the extracellular matrix (ECM) of connective tissues [3,4]. Upon a crosslinking reaction, HA becomes a hydrogel by randomly interconnected HA chains. These structural modifications are possible due to the functional groups present in its

structure. These HA-based hydrogels have been used for different applications, such as controlled release system [5,6], for directing the osteogenic differentiation of human mesenchymal stem cells (MSCs) [7], for tissue engineering [8], and others.

Generally, chemical or physical modification of native HA has been explored to maintain the HA biological functions and to overcome problems related to the degradation of HA-based hydrogels [9,10]. One of these chemical modifications is the partial oxidation of the hydroxyl groups of HA, which is catalyzed by periodate (IO_4^-). This oxidation is used for the introduction of highly flexible links in the otherwise rather stiff and extended structures [11-13] allowing for additional crosslinking with small molecules, such as adipic acid dihydrazide (ADH), thus forming an injectable and biocompatible hydrogel (oxi-HA/ADH) suitable for regenerative medicine [12,14-16]. Oxi-HA/ADH hydrogel has the potential to be used for tissue engineering applications, considering its short gelation time at body temperature, the ease of injection through small gauge needles, and the simplicity of the filtration sterilization methods [12,17].

oxi-HA/ADH hydrogels have been successfully used as controlled drug delivery systems: Jia et al. (2004) showed that oxi-HA/ADH hydrogels are an effective means of delivery of anesthetic bupivacaine to prolong the duration of the sciatic nerve blockade [16]; oxi-HA-ADH hydrogels combined with poly(lactic-co-glycolic acid) (PLGA) nanoparticles were used as drug delivery system by Yeo et al. (2006) to prevent formation of postoperative peritoneal adhesions [15]. More recently, Liang et al. (2018) showed that oxi-HA-ADH hydrogel enables a sustained release of the anti-cancer drug carboplatin and facilitates a synergistic effect with radiotherapy [18]. Liao et al. (2019) [19] incorporated vancomycin

into an oxi-HA-ADH hydrogel and evaluated the antibiotic release and its activity against *S. aureus*.

Nanoporous silicon (nPSi), which consists of silicon nanocrystals embedded in an amorphous porous matrix, is an excellent biomaterial and drug delivery system given its biocompatibility, biodegradability and bioresorbability [20]. Due to its high surface area (typically from 200 to 800 m²/g) [21], surface modification of nPSi is probably the most common route followed for the successful development of nPSi-based drug-delivery systems. However, if it is combined with biopolymers, it can provide new advantageous chemical and physical characteristics, which are not exhibited by the individual constituents, such as an improved control over drug release kinetics and enhanced stability in aqueous solutions [21]. In that sense, in this work nPSi microparticles at concentrations ranging from 0.1% to 1% *m/v* were embedded into oxi-HA/ADH hydrogel for enhanced controlled drug delivery and improved mechanical resistance. Rose Bengal (RB) was used as a model drug because several studies have shown that RB has a cytotoxic effect without irradiation in different cancer cell lines and tumors, such as skin, breast, ovarian, gastric and colon cancer, without affection of healthy cells [22]. The cytocompatibility of nPSi microparticles embedded into oxi-HA/ADH hydrogel was evaluated using fibroblast cell culture.

2. Materials and methods

2.1. Materials and reagents

Hyaluronic acid (HA) with an average molecular weight of 9.48×10^5 Da was purchased from Tops Shandong Topscience Biotech Co. (Rizhao, China). Sodium periodate (NaIO₄), ethylene glycol, adipic acid dihydrazide (ADH), dimethyl sulfoxide (DMSO), Rose

Bengal (RB, MW \approx 1017.64 g/mol), 3-(4,5-dimethylthiazol-2-yl)-2,5-diphenyltetrazolium bromide (MTT) and phosphate buffer solution (PBS) 0.01 M (0.138 M NaCl, 0.0027 M KCl, pH = 7.4 at 25 °C) were purchased from Sigma-Aldrich Inc., (Saint Louis, Missouri, USA). Dialysis membranes with a nominal molecular weight cut-off (MWCO) of 12,000–16,000 DA were sourced from Inlab (Diadema, Brazil). Acetone (C₃H₆O), isopropanol (C₃H₇OH), ethanol (EtOH, C₂H₅OH), hydrogen peroxide (H₂O₂), and hydrofluoric acid (HF) were acquired from Merck, S. A., (Santiago, Chile). All chemicals were used without further purification, and solutions were prepared using Milli-Q water with a resistivity of 18.2 M $\cdot\Omega\cdot$ cm (pH = 7.6). Silicon (Si) wafers (p+ type, boron-doped, orientation <100> resistivity of 0.001–0.005 $\Omega\cdot$ cm) were purchased from University Wafer, South Boston, MA, USA.

2.2. Sample preparation

2.2.1. Synthesis of oxidized hyaluronic acid

Oxidized hyaluronic acid (oxi-HA) was synthesized according to França et al. (2019) [12]. Briefly, hyaluronic acid (HA) with a concentration of 1% (*m/v*) was dissolved in double-distilled water at room temperature, and then an aqueous periodate (NaIO₄) solution (10.67%) was added. The reaction was performed at room temperature for 24 h in the dark. The reaction was stopped by the addition of ethylene glycol for half an hour. The resulting solution was dialyzed with double-distilled water for three days by using a semipermeable membrane (with a MWCO of 12–16 kDa). Finally, the dialyzed solution was lyophilized, yielding a white fluffy product. The obtained oxidation degree was 65 \pm 4% [12].

2.2.2. Synthesis of nanoporous silicon microparticles

Si wafers were cleaned by ultrasonication in acetone, isopropanol and distilled water, for a period of 15 min in each solvent. Acetone removed greasy and oily substances;

isopropanol was necessary to rinse acetone off, and distilled water removed any isopropanol residues. Then, nanoporous silicon (nPSi) layers were fabricated by electrochemical etching from the cleaned Si wafers in HF (48%):EtOH (1:2) solution under controlled formation conditions: etching time of 30 min and current density of 80 mA/cm². Afterwards, an electropolishing pulse was applied to get free-standing nPSi layers. For that, the applied current density was increased up to 150 mA/cm² during 2 s. nPSi free-standing layers were scraped with a diamond tip to obtain particles. They were milled, collected in EtOH and subjected to 10 min ultrasonic agitation for homogenization; milled and ultrasonically re-suspended again. Then, the suspended nPSi microparticles in the solution were collected by decantation and chemically oxidized with H₂O₂ (30%, v/v) for 12 h in orbital agitation. Finally, microparticles were rinsed with EtOH and dried.

2.2.3. Synthesis of oxi-HA/ADH hydrogels with or without nPSi microparticles

oxi-HA was dissolved overnight in phosphate buffer saline solution (PBS) (pH 7.4, at 4 °C) to obtain a final concentration of 6% (m/v). Then, 8% (m/v) of the ADH solution was prepared in PBS at 4°C. The oxi-HA was mixed with nPSi particles in different low concentrations (m/v): 0% (control), 0.1%, 0.5% and 1.0%. Mixtures were homogenized using a vortex for 1 min. Afterward, the oxi-HA solutions, with or without nPSi microparticles, and ADH solution were mixed in proportion 4:1 (oxi-HA:ADH) to form the samples: oxi-HA/ADH (control), oxi-HA/ADH with 0.1% nPSi, oxi-HA/ADH with 0.5% nPSi and oxi-HA/ADH with 1.0% nPSi. The reaction took place at 5 °C for 24 h in the dark. The obtained hydrogels presented a diameter of 9 mm and a height of 4 mm.

2.3. Characterization

2.3.1. Microscopic characterization

Micrographs of samples were obtained on a Nikon optical microscope (Melville, NY, USA). The nanopores of the nPSi microparticles were observed by a variable pressure scanning electron microscope (VP-SEM, SU-3500 Hitachi, Tokyo, Japan) using an acceleration voltage of 10 kV. Hydrogels were freeze-dried using liquid nitrogen and their morphology was observed by SEM (LEO 440i, Cambridge, England) using an acceleration voltage of 10 kV.

2.3.2. Physicochemical characterization

The size distribution, polydispersity index (PDI) and zeta potential of nPSi microparticles were quantified by dynamic light scattering using a Zetasizer Nano ZS (Malvern Panalytical, United Kingdom). The measurements were performed in triplicate using a Ne-He laser and a scattering angle of 90°. The concentration of samples was 0.1 % (m/v) at 25°C.

For optical properties analysis, UV-Vis absorbance spectra were recorded using a Jasco V-750 double-beam spectrophotometer (Hachioji, Tokyo, Japan). Attenuated Total Reflectance Fourier-Transform Infra-Red Spectroscopy (ATR-FTIR) was used for chemical analyses of the microparticles. An FTIR spectrometer (CARY 630 FTIR Agilent Technologies, USA) was used in a range between 4000 and 600 cm^{-1} with a resolution of 1 cm^{-1} (NS = 4). The obtained spectra were mathematically processed by data smoothing and normalization.

Crystallographic structures of the samples were examined by X-ray Diffraction (XRD) using a Rigaku X-ray diffractometer Smartlab model, with goniometer Theta-Theta Bragg-Brentano geometry and solid-state detector D/teX Ultra 250 model (Rigaku Corporation, Japan). The instrumental alignment was checked against the NIST SMR 660c LaB6 powder standard and Ni-filtered Cu radiation (30 kV and 40 mA) was employed. The

optical configuration included a 0.5° divergence slit, a 0.25° anti-scatter slit, and both sides with 5° Soller slits. In preference, patterns were collected in the 15–65° range, counting 0.5°/s per step of 0.01°.

2.3.3. Mechanical tests and hydrolytic degradation tests

The mechanical properties of hydrogels, compressive force and stress strength, were measured using a TA.XT2 texturometer (Stable Micro Systems, Godalming, UK) with a 50 N load cell at room temperature. The speed test was 0.2 mm/s. The hydrogels were subjected to a compressive force of up to 70%.

Hydrolytic degradation tests were conducted in PBS (pH 7.4) at 37 °C using the gravimetric method. Mass loss measurements of the hydrogels in PBS was calculated with degradation time using equation 1 [23]:

$$\text{Residual mass (\%)} = \left(\frac{M_i - M_f}{M_i} \right) \times 100\% \quad (1)$$

where M_i is the initial mass of the sample and M_f is the final mass of the degraded sample extracted at each time period.

2.4. Drug release profiles

2.4.1. Rose Bengal loading

nPSi particles were loaded with Rose Bengal (RB, 0.001 M, pH 5.5) for 15 min at 50 RPM and room temperature, followed by three consecutive Milli-Q water rinse steps of 5, 3 and 1 min, respectively. The pH of the water rinse was previously adjusted at 5.5. In the case of pure hydrogels, RB was directly incorporated during synthesis as it was described in section 2.2.3., but nPSi% was substituted for RB%. Other hydrogel series consisted of nPSi

previously loaded with RB and incorporated into the hydrogel to obtain the samples according to what stated in section 2.2.3.

2.4.2. Rose Bengal release

To determine the release profiles, RB loaded samples were placed into vials filled with PBS (37 °C) in a horizontal shaker at 100 RPM (NB-2005LN Biotek, Winooski, VT, USA). At predetermined time intervals, RB was detected using a Thermo Scientific Evolution-220 spectrophotometer (Waltham, Massachusetts, USA) at 545 nm [24]. All experiments were conducted in triplicate and non-loaded samples were used as controls in these kinetic experiments.

In order to determine the mechanism of drug release, the model Korsmeyer-Peppas model was fitted to the release profiles. The Korsmeyer-Peppas semi-empirical model is given by [25]:

$$M_t/M_\infty = k_{KP} \cdot t^n \quad (2)$$

where M_t/M_∞ is the fractional drug release, t is the release time, k_{KP} is the Korsmeyer-Peppas release kinetic constant characteristic of the drug/system and n is an exponent which characterizes the mechanism of release [25]. The fitting of the model was conducted with OriginLab software.

2.5 Cytotoxicity and cell viability assays

2.5.1. Cell culture

The BALB/c 3T3 (murine fibroblast) cell line was cultured in plastic flasks with Dulbecco modified Eagle's minimal essential medium (DMEM), supplemented with 10% inactivated fetal bovine serum (FBS) and 1% antibiotic solution (penicillin and streptomycin,

P/S). The cultures were incubated at 37°C in an atmosphere containing 5% CO₂. The medium was changed every 72 hours.

2.5.2. MTT reduction assays

For cytotoxicity assays, cells were distributed in 24-well plates using a density of 5×10^4 cell/mL and were incubated at 37°C at 5% CO₂ for 24 hours. Later, the cells were treated with different concentrations (0 to 2.5 mg/mL) of nPSi microparticles for 72 hours. After incubation, the medium was removed, wells were washed with PBS, and 200 µL of 3-(4,5-dimethylthiazol-2-yl)-2,5-diphenyltetrazolium bromide (MTT) solution (1 mg/mL) was added to each well. The plate was incubated for 3 h at 37°C, MTT solution was removed and the formazan crystal was solubilized in 1 mL of dimethyl sulfoxide (DMSO). The plate was shaken for 5 min and the absorbance of each well was read using an Infinity M200Pro spectrophotometer (Tecan, Männedorf, Switzerland). The measured absorbance at $\lambda = 570$ nm was normalized to the value obtained for the control: cells were cultured without samples [18].

For cell viability assays, the hydrogels with or without different nPSi were prepared in a 48-well plate. Briefly, 240 µL of oxi-HA with nPSi microparticles was added in each well, and gelation was induced with 60 µL of 8% ADH. After gelation, 700 µL of DMEM with FBS and P/S were added and incubated at 37°C at 5% CO₂ for 24 h. Cells were seeded using a density of 2×10^4 cell/mL and were incubated at 37°C at 5% CO₂ for 3 or 6 days. After incubation, the medium was removed, wells were washed with PBS, and 200 µL of MTT solution (1 mg/mL) was added to each well. The plate was incubated for 4 h at 37°C, MTT solution was removed and the formazan crystal was solubilized in 0.5 mL of DMSO. The plate was shaken for 30 min and the absorbance of each well was read in the spectrophotometer (Infinity M200Pro, Tecan, Männedorf, Switzerland). The measured

absorbance at $\lambda = 570$ nm was normalized to the value obtained for the control: cells were cultured without samples [26].

2.5.3. Statistical analysis

Each experiment was carried out in triplicate unless otherwise specified. All the results are presented as the mean \pm standard deviation (SD). The experimental data from all the studies were analyzed using analysis of variance (ANOVA). The statistical significance was set to p-value ≤ 0.05 .

3. Results and discussion

The synthesized nPSi particles are shown in the scanning electron microscopy (SEM) image of Figure 1A. Microparticles are characterized by columnar-like pores with an average pore diameter of 50 nm. Moreover, these particles had a spike-like structure with around 1 μ m width, and a length ranging from 1 μ m to 5 μ m. The size of particles was also measured by dynamic light scattering (DLS), and the obtained size distribution is shown in Figure 1B. Measurements resulted in an average diameter of 825 nm, which is close to the size of particles observed by SEM. The obtained polydispersity index (PDI) was 0.9018 ± 0.0141 , denoting the wide size polydispersity of the nPSi structures.

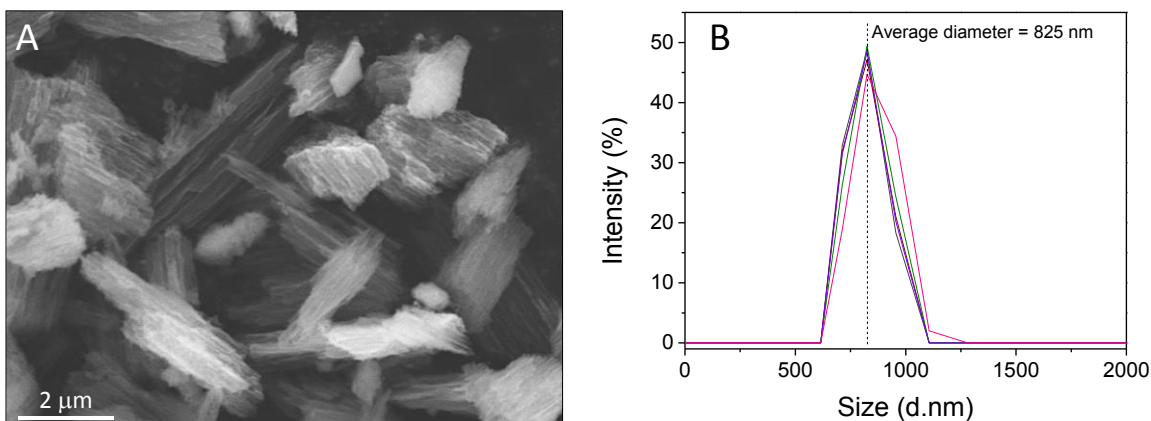


Figure 1. A) SEM image of nPSi microparticles. B) Particle size distribution.

In order to stabilize the surface and pores of the nPSi, microparticles were chemically oxidized by H_2O_2 [27]. Due to this process, the obtained zeta potential value of microparticles was -15.30 ± 0.54 mV, which stems from the negatively charged Si-O-Si and Si-OH groups generated by the chemical oxidation [27].

According to França et al. (2019) [12], oxidized hyaluronic acid (oxi-HA) was crosslinked with adipic acid dihydrazide (ADH) to obtain the oxi-HA/ADH hydrogel (Figure 2). This protocol was modified to embed nPSi microparticles into the hydrogel using three m/v concentrations: 0.1, 0.5 and 1.0 m/v % nPSi. Figures 3A-3D show optical microscopy images of the composites. The physical appearance of hydrogels samples became significantly darker by increasing the concentration of nPSi. In fact, some regions with agglomerated particles could be observed, which agrees with a zeta potential higher than -30 mV [28]. It is well known that the range of zeta potentials for fully suspended silica based colloidal systems is higher than $+30$ mV or lower than -30 mV. Additionally, representative images are presented as insets. On the other hand, samples were freeze-dried using liquid nitrogen to explore the internal structure of hydrogels by SEM (Figures 3E-3H). In all

hydrogels, a three-dimensional skeleton with interconnected and semi-rounded pores was observable. Control oxi-HA/ADH samples presented pores of around 100 μm of diameter, which were reduced when the nPSi concentration increased. The pore diameter of oxi-HA/ADH w/1.0% nPSi was reduced down to 30 μm .

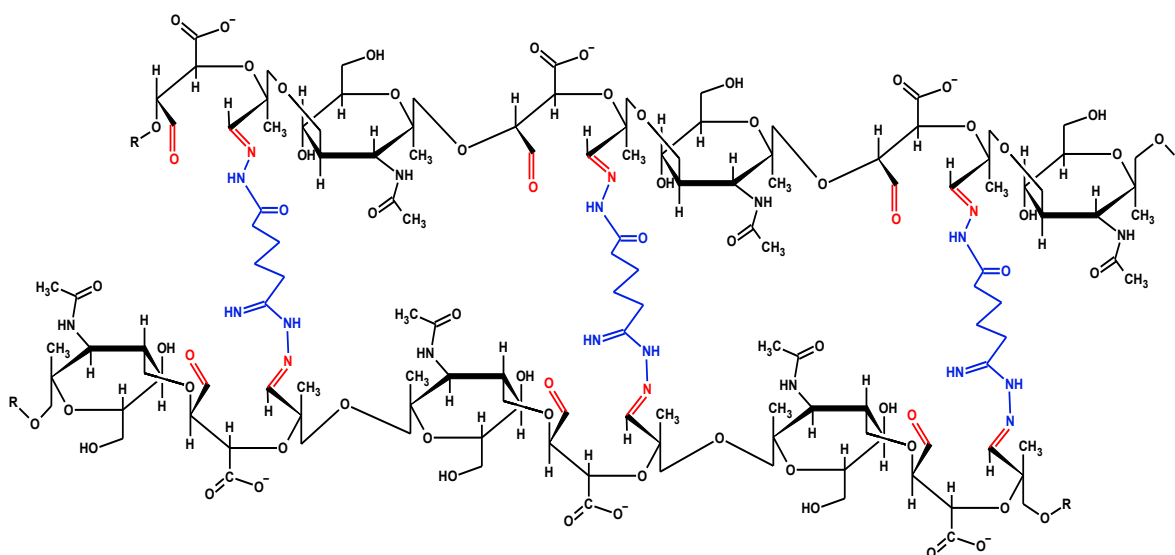


Figure 2. Chemical structure of oxi-HA/ADH hydrogel.

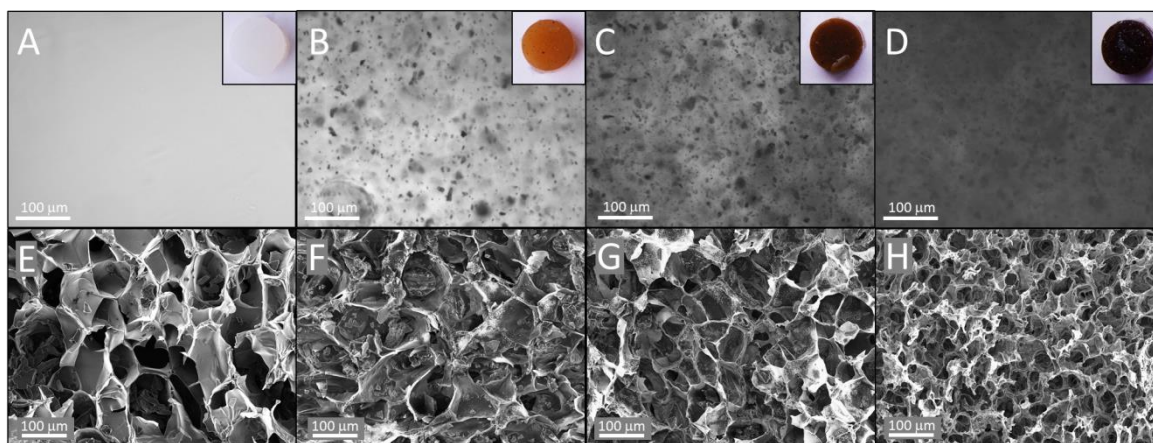


Figure 3. Optical microscopy images of hydrogels: A) oxi-HA/ADH, B) oxi-HA/ADH with 0.1% nPSi, C) oxi-HA/ADH with 0.5%, and D) oxi-HA/ADH 1.0%. Insets are representative images of each cylindrical sample ($\varnothing \approx 9 \text{ mm}$, $h \approx 4 \text{ mm}$). SEM images of

hydrogels: E) oxi-HA/ADH, F) oxi-HA/ADH with 0.1% nPSi, G) oxi-HA/ADH with 0.5% nPSi, and H) oxi-HA/ADH with 1.0% nPSi.

UV-Vis analysis is presented in Figure 4A. oxi-HA/ADH spectrum showed an absorbance almost zero in the visible range (380 to 780 nm) because the hydrogel is quasi-transparent. However, when the nPSi concentration was increased, the absorbance increased due to the opacity of the microparticles. On the other hand, FTIR analyses were performed to evaluate the chemical composition of samples (Figure 4B). In that sense, the nPSi spectrum exhibited a band at 795 cm^{-1} , which corresponds to the characteristic vibration of the Si–OH bond [29]. The bands related to surface Si–O–Si stretching mode at 1200 and 1052 cm^{-1} were also observed [30,31]. These results are in agreement with oxidized nPSi microparticles and in agreement with the obtained negative zeta potential value. The oxi-HA/ADH spectrum exhibited bands corresponding to different functional groups that are according to the molecular structure of oxi-HA/ADH (Figure 2) [12,30]. Additionally, those bands were also identified in the hydrogels with nPSi. The C–OH stretching mode was detected at 1003 cm^{-1} , which was shifted to higher wavenumber in the samples with nPSi due to the Si–O–Si band of nPSi microparticles (1052 cm^{-1}). This suggests a chemical interaction between oxi-HA/ADH and nPSi. In the case of the bands at 1372 cm^{-1} , 1534 cm^{-1} , 1648 cm^{-1} and 2925 cm^{-1} , they can be attributed to the CH_3 symmetric bending, C–N stretching, secondary amide N–C=O stretching and C–H stretching vibration, respectively. Wide band at 3250 cm^{-1} is attributed to O–H stretching of hydroxyl groups, and to N–H stretching of secondary amides, which was also replicated at 1615 cm^{-1} . According to these results, the binding between the nPSi microparticles and oxi-HA/ADH hydrogel can be understood by different phenomena. Firstly, as nPSi microparticles were oxidized, oxi-HA easily permeated into the porous

structures. Then, when oxi-HA was cross-linked by ADH, electrostatic interactions between negatively Si-OH and Si-O-Si bonds of nPSi with positively nitrogenated bonds of oxi-HA/ADH hydrogel were formed. Additionally, hydrogen bonding could be involved in further interactions with the pore walls and the porosity of microparticles could also work as a mechanical (stress) anchoring system.

In order to characterize the crystalline nature of the nPSi microparticles embedded into the hydrogels, samples were analyzed by X-ray diffraction (XRD) (Figure 4C). Diffractogram of nPSi revealed their characteristic peaks of Si corresponding to the (111), (220), and (311) crystallographic plane at 27.9°, 46.6° and 55.2°, respectively [32]. The low intensity and high broadness of the peaks is due to the small nanocrystallite size in nanoporous dust, in agreement with previously inside nPSi sponge structures [32]. However, when nPSi was embedded into hydrogels, peaks slightly shifted to higher two theta values, and the intensity of peaks increased according to nPSi concentration. This could be due to a rise in the average size distribution of Si crystallites (by volume) because the smallest nanocrystals got oxidized during hydrogel-nPSi composite formation [32].

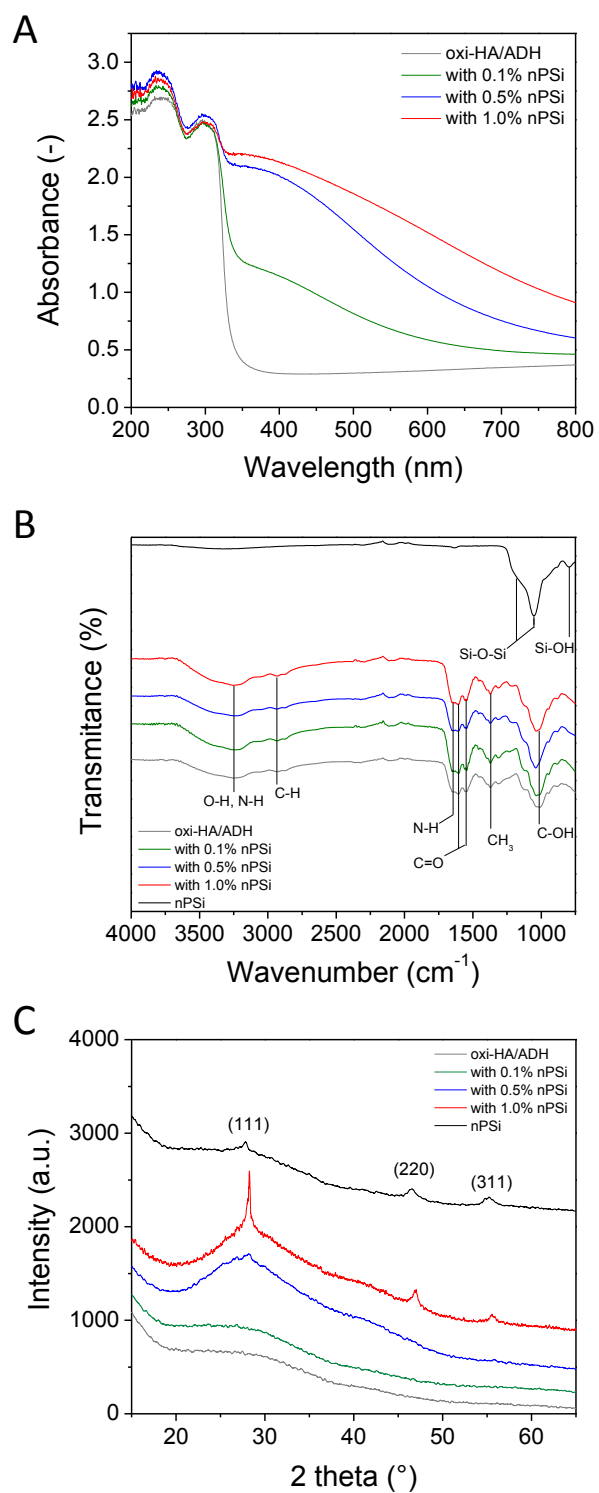


Figure 4. A) UV-Vis spectra of hydrogels, B) FTIR-ATR spectra of hydrogels, and C) XRD analysis of hydrogels.

The effects of nPSi incorporation on the mechanical properties of the hydrogels were studied by measuring the compressive force and stress strength (Figure 5A and Figure 5B, respectively). As expected, hydrogels were more resistant when the nPSi concentration was increased. For both studies, compressive force and stress strength tests, samples with 1% nPSi doubled the values of control samples. The compression force obtained by oxi-HA/ADH was 3.50 ± 0.03 N and increased up to 7.03 ± 0.18 N in the sample HA/ADH with 1% nPSi. In the case of stress strength, values went from 0.017 ± 0.001 to 0.035 ± 0.001 MPa for above mentioned samples, respectively. Higher mechanical resistance of hydrogels with nPSi microparticles was due to the inorganic characteristic of the nPSi, but it could be also induced by the modification of the internal three-dimensional skeleton of hydrogels. As it was observed in the SEM images of Figure 3, polymer interconnections became shorter and denser due to nPSi microparticles distribution into the hydrogel. The higher mechanical resistance of hydrogels achieved by nPSi microparticles incorporation had an effect in the stability of samples immersed in PBS. Figure 5C shows the hydrolytic degradation kinetics of samples in PBS at 37 °C. The hydrolytic degradation profiles, in terms of the remaining mass fraction, exhibited similar behavior along time. However as in the previous mechanical resistance tests, hydrogels were more stable for increasing concentrations of nPSi particles. For example, at day 31 samples presented $24 \pm 3\%$, $28 \pm 3\%$, $30 \pm 2.5\%$ and $33 \pm 2\%$ residual mass for oxi-HA/ADH (control), oxi-HA/ADH with 0.1% nPSi, oxi-HA/ADH with 0.5% nPSi and oxi-HA/ADH with 1.0% nPSi, respectively.

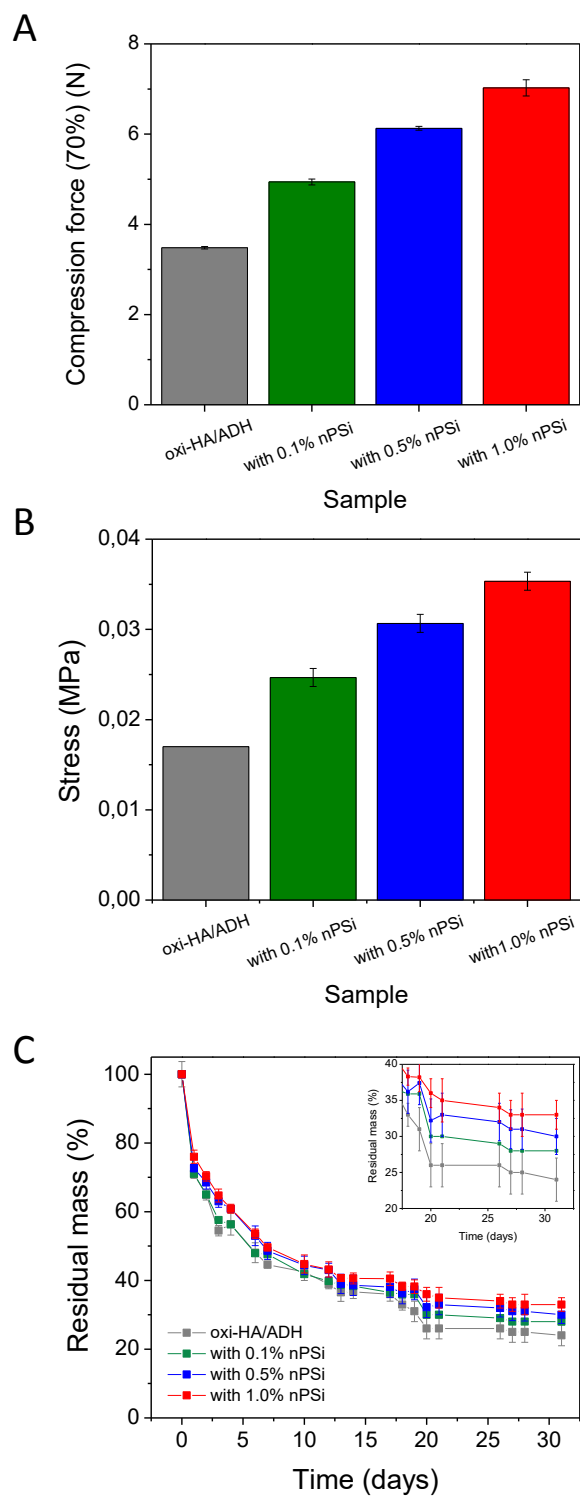


Figure 5. Mechanical properties of the hydrogels: A) Compressive force, and B) Stress strength. C) Residual mass as a function of hydrolysis time (PBS medium at pH 7.4 and 37 °C).

348

349 In order to evaluate the drug delivery functionality of hydrogels, samples were tested
350 with RB in PBS batches at 37 °C under stirring. RB release profiles are shown in Figure 6
351 and kinetic parameters obtained from the analysis of the profiles are detailed in Table 1. nPSi
352 microparticles were loaded with a high concentrated aqueous solution of RB, obtaining a
353 maximum release of 99 ± 1 μg RB/mg nPSi at 24 h (Figure 6A). In the case of the control
354 hydrogel (oxi-HA/ADH), RB was directly incorporated into the samples at three different
355 %RB (*m/v*) concentrations: 0.1%, 0.5% and 1.0% RB (Figure 6B). As expected, the total
356 amount of released RB increased according to the initial RB load: 0.055 ± 0.001 μg RB/mg
357 for oxi-HA/ADH with 0.1% RB, 0.255 ± 0.040 μg RB/mg for oxi-HA/ADH with 0.5% RB
358 and 2.55 ± 0.25 μg RB/mg for oxi-HA/ADH with 1.0% RB, all of them at 24 h. These results
359 indicate a 3.33% release of RB from the initial RB load for oxi-HA/ADH with 0.1% and
360 0.5% RB. For the case of oxi-HA/ADH with 1.0 % RB, the percent of RB released from the
361 initial RB load was 16.2%. This indicates that most of the RB remained stacked into the
362 hydrogels. Figure 6C shows the RB release profiles from hydrogels with nPSi. That is to say,
363 RB was previously loaded in nPSi microparticles and then incorporated into the hydrogels.
364 In this series, samples reached the maximum RB release in up to 72 h (not shown in the plot)
365 with values of: 0.030 ± 0.002 , 0.150 ± 0.007 and 0.150 ± 0.007 μg RB/mg for oxi-HA/ADH with
366 0.1%, 0.5% and 1.0% nPSi, respectively. Evidently, the absolute release from these samples
367 was significantly lower than the obtained for pure oxi-HA/ADH because the initial RB
368 loading capacity was restricted to the nPSi. However, the normalized RB release amounts
369 were higher: 17.9%, 16.6% and 14.5% for oxi-HA/ADH with 0.1%, 0.5% and 1.0% nPSi,
370 respectively.

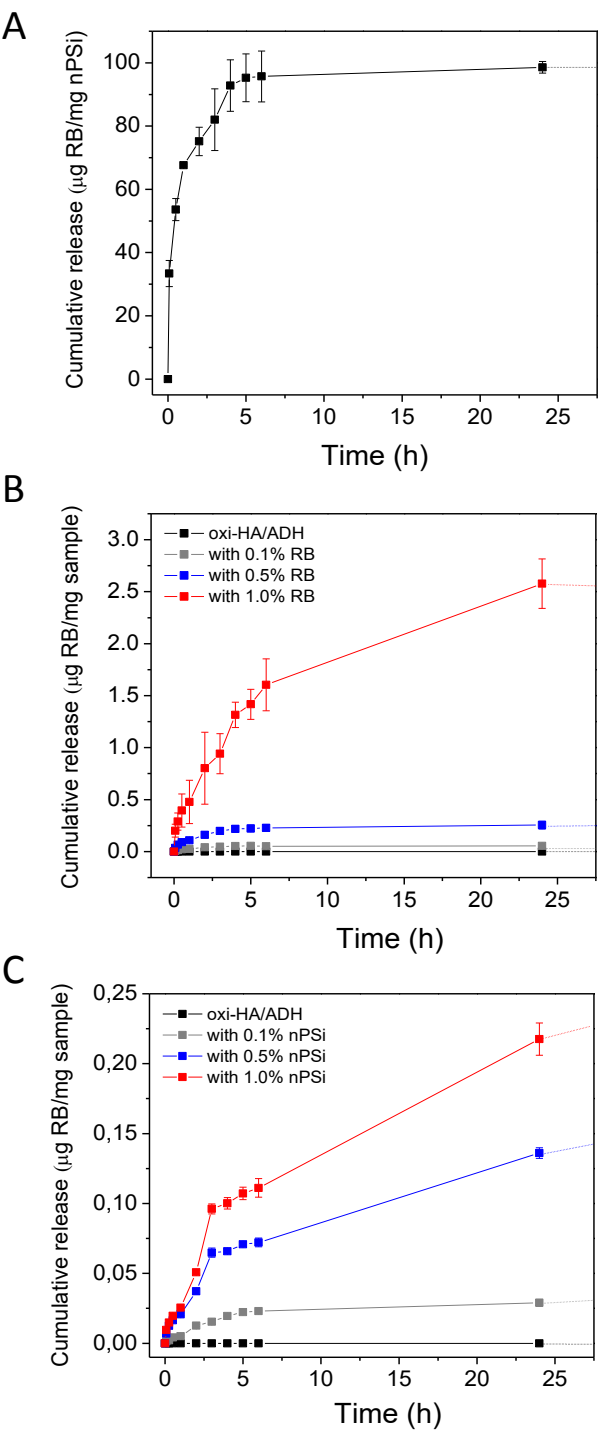


Figure 6. RB release profiles: A) nPSi microparticles, B) pure oxi-HA/ADH hydrogel with different RB%, and C) oxi-HA/ADH hydrogel with different nPSi%, which was previously loaded with RB.

To attain a deeper perception of the mechanisms that govern the release of RB from the samples, release profiles were fitted to the Korsmeyer-Peppas model (Figure 7) because this one is valid for different geometries, such as cylinder, and fits for early time of release [33]. As RB release profiles were normalized, it is appreciable that RB release from pure oxi-HA/ADH hydrogels presented considerable data dispersion (Figure 7B). However, in the case of nPSi and hydrogels with nPSi (Figure 7A and 7C, respectively), the release data were less dispersed. According to the obtained k_{KP} values, which are related to drug/carrier interaction and rate of release [34], RB presented the next rate tendency: nPSi > pure hydrogel series > hydrogel with nPSi series. Although nPSi showed the higher RB loading (Table 1) due to its large surface area [27], it presented the fastest release because it was not specifically to immobilize RB. In the case of pure oxi-HA/ADH series, RB release was slower than nPSi microparticles due to the hydrogel–RB interactions across the network [35]. For the oxi-HA/ADH with nPSi series, RB exhibited even slower release than pure oxi-HA/ADH because RB diffused first from nPSi to hydrogel matrix, and afterward, from hydrogel network to PBS medium. Although the Korsmeyer-Peppas model is limited for early time of release, it is useful to determine the release mechanism, even if one or more types of phenomena of drug release are involved. It can be seen, as a generalization of the observation of the superposition of apparently independent mechanisms of drug transport, relaxation, and diffusion, which are identified depending on the obtained n value [33]. RB release from nPSi, and from oxi-HA/ADH hydrogels with 0.1% and 0.5% RB, presented n

values lower than 0.45. When the Korsmeyer–Peppas is applied to cylindrical geometries, as the studied samples, the release exponent $n \leq 0.45$ [33], corresponds to a Fickian diffusion release during which the solvent penetration is the rate-limiting step. The rest of samples, oxi-HA/ADH with 1.0% RB and all the oxi-HA/ADH with nPSi, showed n values in the range $0.45 < n < 0.89$. For cylindrical geometries, this means that release is related to non-Fickian or anomalous transport, and the mechanism of drug release is governed by diffusion and swelling. In the case of the oxi-HA/ADH with nPSi series, the swelling could be explained by the large surface area and porosity of nPSi; as RB diffuses, water molecules are adsorbed leading to swelling of the hydrogel. In the case of oxi-HA/ADH with 1.0% RB, the mass of RB was large enough to induce the same effect.

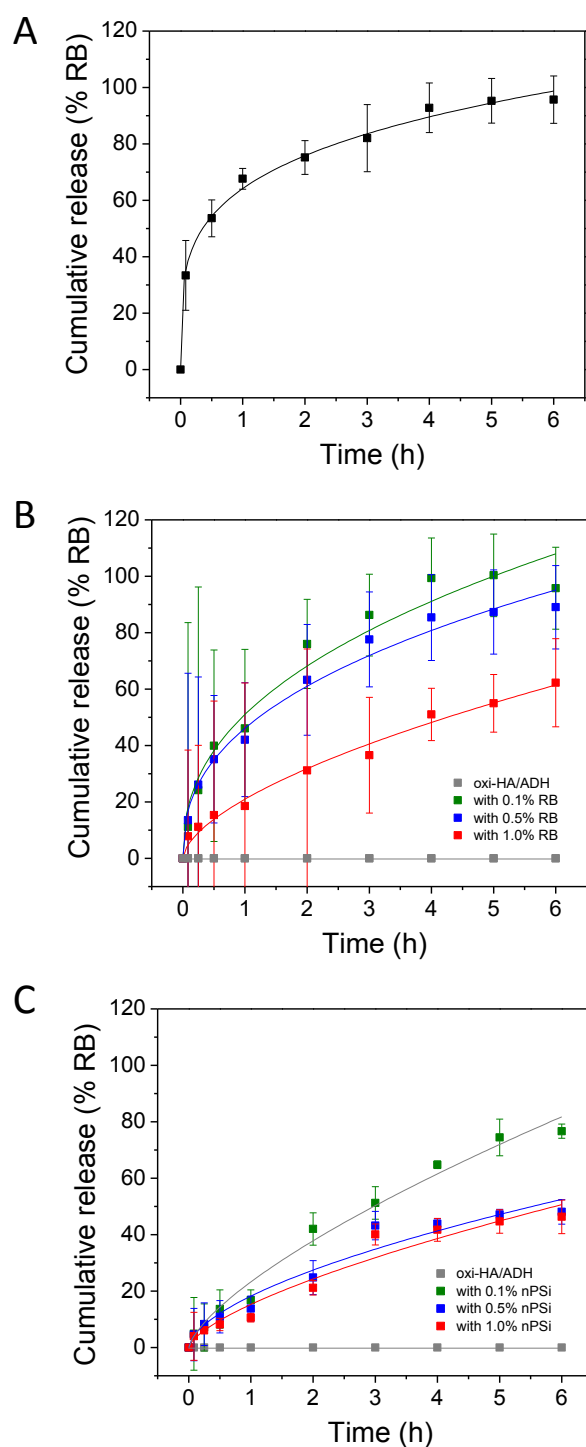


Figure 7. Korsmeyer-Peppas model fitting of RB release profiles: A) nPSi microparticles, B) pure oxi-HA/ADH hydrogel with different RB%, and C) oxi-HA/ADH hydrogel with different nPSi%, which was previously loaded with RB.

411

412

Table 1. *In-vitro* release kinetics of Rose Bengal in PBS at 37 °C.

Sample	RB in sample initially (µg/mg)	RB released from initial load (%)	RB released (µg/mg)	Korsmeyer-Peppas model		
				$\frac{M_t}{M_\infty} = k_{KP} t^n$		
				$k_{KP}(h^{-n})$	n	r_{adj}^2
nPSi	101.0±3.0	98.0±1 at 24 h	99±1 at 24 h	64.1723	0.2405	0.9946
oxi-HA/ADH	-	-	-	-	-	-
with 0.1% RB	1.67±0.13	3.33±0.54 at 24 h	0.055±0.001 at 24 h	51.002	0.4186	0.9658
with 0.5% RB	8.17±0.52	3.33±0.47 at 24 h	0.255±0.040 at 24 h	46.1206	0.4042	0.9855
with 1.0% RB	15.98±2.09	16.2±1.60 at 24 h	2.55±0.25 at 24 h	20.9826	0.5997	0.9876
with 0.1% nPSi	0.168±0.001	17.9±1.5 at 72 h	0.030±0.002 at 72 h	23.2571	0.7018	0.9853
with 0.5% nPSi	0.905±0.030	16.6±1.0 at 72 h	0.150±0.007 at 72 h	18.2185	0.5907	0.9585
with 1.0% nPSi	1.720±0.054	14.5±1.0 at 72 h	0.250±0.014 at 72 h	15.2761	0.6687	0.9541

413

414

415 To evaluate the cytotoxic effect of nPSi microparticles, fibroblast cells were cultured

416 (Figure 8A). Results showed that viability gradually decreased and responded in a

417 concentration-dependent manner. Cell viability was slightly reduced from 100% to 95% for

418 concentrations of bare nPSi microparticles from 0 to 0.25 mg/mL, while surviving cells were

419 77% for concentration of 0.50 mg/mL. For concentrations equal or upper to 1.5 mg/mL,

420 surviving cells dropped down to ≤27%. On the other hand, the cell viability of hydrogels with

421 nPSi was tested also with fibroblast cell culture. The initial cell density (ICD) seeded was

422 2×10^4 cell/mL and replicas were incubated for 3 and 6 days (Figure 8B). After the third day

423 of cell culture, oxi-HA/ADH increased 2.5 times the ICD, and oxi-HA/ADH with 0.1% nPSi

424 and oxi-HA/ADH with 0.5% nPSi practically kept the same value of 2×10^4 cell/mL. Just a

425 slight decrease of 15% was detected in the oxi-HA/ADH hydrogel with 1.0% nPSi.

426 Nevertheless, after the 6th day, pure oxi-HA/ADH increased the cell density up to more than

six times. In the case of the three hydrogels with nPSi, they went over a two-fold increase of the ICD value. Therefore, the behavior during the first days can be considered as temporary inhibition of cell proliferation due to adaptation mechanisms of the cells to this kind of material. On the other hand, in terms of concentration (m/v), 0.1% nPSi is equivalent to 1 mg/mL, 0.5% nPSi is equivalent to 5 mg/mL and 1.0 % nPSi is equivalent to 10 mg/mL. In that sense, we can say that the tolerance of fibroblast cells to nPSi microparticles could be considerably higher than 1.5 mg/mL due to the oxi-HA/ADH hydrogel.

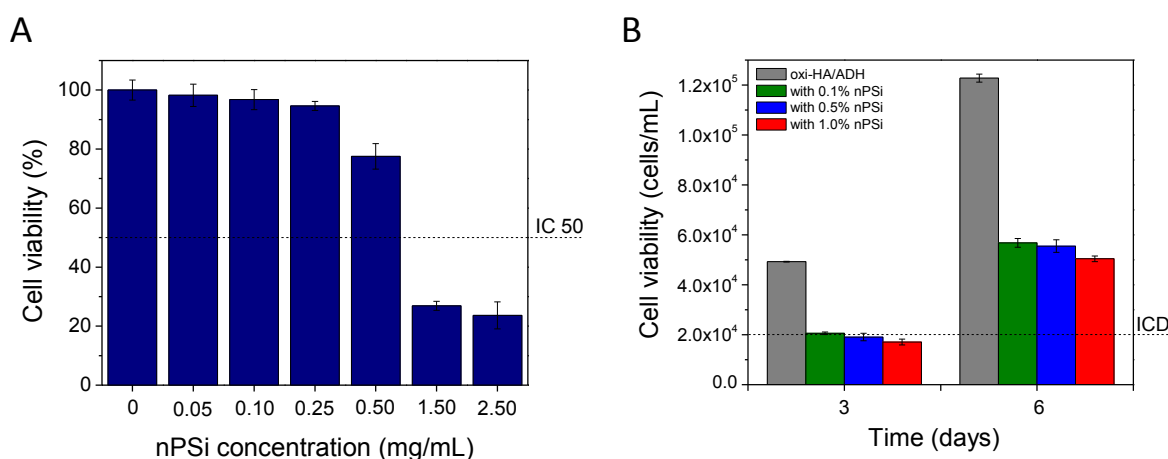


Figure 8. A) Cytotoxicity of nPSi microparticles. B) Cell viability of hydrogels.

4. Conclusions

Microparticles of nPSi with a columnar-like pore morphology were obtained. They showed an average pore diameter of 50 nm and a length that went from 1 to 5 μ m. These microparticles were successfully embedded into oxi-HA/ADH when the crosslinking between HA and ADH was performed. Then, electrostatic interactions between negatively Si-OH and Si-O-Si bonds of nPSi with positively nitrogenated bonds of oxi-HA/ADH hydrogel were formed. Additionally, hydrogen bonding could be involved in pore walls and

porosity of microparticles could also work as a mechanical anchoring between the microparticle-hydrogel composite. Our results showed that oxi-HA/ADH hydrogel with only 1% *m/v* nPSi microparticles induced a two-fold increase of both compressive force and stress strength with respect to the pure hydrogel formulation. On the other hand, to evaluate the drug delivery functionality of hydrogels, samples were loaded with RB as a model drug. Samples of oxi-HA/ADH with nPSi microparticles (from 0.1 % to 1% *m/v*) improved the control over RB release kinetics with respect to the direct release from pure oxi-HA/ADH hydrogel. Finally, the cytocompatibility of nPSi microparticles and the cell viability of nPSi microparticles embedded into oxi-HA/ADH hydrogel were confirmed using fibroblast cell culture up to 6 days, denoting no adverse reactions, although the proliferation rate was lower than for oxi-HA/ADH hydrogel controls.

Author's contributions

CGF and JHM conceived and designed experiments; TP and GR synthesized the nPSi microparticles; CGF and TP synthesized hydrogels and hydrogels with microparticles; NN and MMS performed the microscopy characterization; CGF and TP performed the physicochemical characterization and mechanical resistance tests; CGF and MHAS performed the biological experiments; CGF and JHM analyzed the data; MHAS, MMS and JHM contributed reagents/materials/analysis tools; CGF and JHM wrote the manuscript. All authors revised the manuscript.

Acknowledgments

This work was financially supported by FONDECYT–Chile (grant number 11180395), CONICYT PFCHA/DOCTORADO/2017-21172001 (Nelson Naveas) and

CNPq140924/2017-5 (Carla França). We thank Dr. Héctor Pesenti for providing the DRX facility (FONDEQUIP–Chile, project 160152), and Dr. Luis Sanhueza for optical measurements of UV-Vis spectroscopy.

Availability of data

The data that support the findings of this study are available from the corresponding author upon reasonable request.

Declaration of interest statement

The authors declare that they have no competing interests.

References

- [1] Maharjan AS, Pilling D, Gomer RH. High and low molecular weight hyaluronic acid differentially regulate human fibrocyte differentiation. *PloS one* 2011;6(10).
- [2] Sahiner N, Suner SS, Ayyala RS. Mesoporous, degradable hyaluronic acid microparticles for sustainable drug delivery application. *Colloids and Surfaces B: Biointerfaces* 2019;177:284-93.
- [3] Jha AK, Hule RA, Jiao T, Teller SS, Clifton RJ, Duncan RL, et al. Structural analysis and mechanical characterization of hyaluronic acid-based doubly cross-linked networks. *Macromolecules* 2009;42(2):537-46.
- [4] Fallacara A, Baldini E, Manfredini S, Vertuani S. Hyaluronic acid in the third millennium. *Polymers* 2018;10(7):701.
- [5] Xu X, Jha AK, Duncan RL, Jia X. Heparin-decorated, hyaluronic acid-based hydrogel particles for the controlled release of bone morphogenetic protein 2. *Acta biomaterialia* 2011;7(8):3050-9.
- [6] Xiao L, Tong Z, Chen Y, Pochan DJ, Sabanayagam CR, Jia X. Hyaluronic acid-based hydrogels containing covalently integrated drug depots: implication for controlling inflammation in mechanically stressed tissues. *Biomacromolecules* 2013;14(11):3808-19.

496 [7] Jha AK, Xu X, Duncan RL, Jia X. Controlling the adhesion and differentiation of
 497 mesenchymal stem cells using hyaluronic acid-based, doubly crosslinked networks.
 498 Biomaterials 2011;32(10):2466-78.

499 [8] Suner SS, Demirci S, Yetiskin B, Fakhrullin R, Naumenko E, Okay O, et al. Cryogel
 500 composites based on hyaluronic acid and halloysite nanotubes as scaffold for tissue
 501 engineering. Int.J.Biol.Macromol. 2019;130:627-35.

502 [9] Hoare TR, Kohane DS. Hydrogels in drug delivery: Progress and challenges. Polymer
 503 2008;49(8):1993-2007.

504 [10] Burdick JA, Prestwich GD. Hyaluronic acid hydrogels for biomedical applications.
 505 Adv Mater 2011;23(12):H41-56.

506 [11] Jia X, Burdick JA, Kobler J, Clifton RJ, Rosowski JJ, Zeitels SM, et al. Synthesis and
 507 characterization of in situ cross-linkable hyaluronic acid-based hydrogels with potential
 508 application for vocal fold regeneration. Macromolecules 2004;37(9):3239-48.

509 [12] França CG, Sacomani DP, Villalva DG, Nascimento VF, Dávila JL, Santana MHA.
 510 Structural changes and crosslinking modulated functional properties of oxi-HA/ADH
 511 hydrogels useful for regenerative purposes. European Polymer Journal 2019;121:109288.

512 [13] Kristiansen KA, Dalheim MØ, Christensen BE. Periodate oxidation and
 513 macromolecular compaction of hyaluronan. Pure and Applied Chemistry 2013;85(9):1893-
 514 900.

515 [14] Su W, Chen Y, Lin F. Injectable oxidized hyaluronic acid/adipic acid dihydrazide
 516 hydrogel for nucleus pulposus regeneration. Acta biomaterialia 2010;6(8):3044-55.

517 [15] Yeo Y, Highley CB, Bellas E, Ito T, Marini R, Langer R, et al. In situ cross-linkable
 518 hyaluronic acid hydrogels prevent post-operative abdominal adhesions in a rabbit model.
 519 Biomaterials 2006;27(27):4698-705.

520 [16] Jia X, Colombo G, Padera R, Langer R, Kohane DS. Prolongation of sciatic nerve
 521 blockade by in situ cross-linked hyaluronic acid. Biomaterials 2004;25(19):4797-804.

522 [17] Su W, Chen K, Chen Y, Lee Y, Tseng C, Lin F. An injectable oxidated hyaluronic
 523 acid/adipic acid dihydrazide hydrogel as a vitreous substitute. Journal of Biomaterials
 524 Science, Polymer Edition 2011;22(13):1777-97.

525 [18] Liang HT, Lai X, Wei M, Lu S, Wen W, Kuo S, et al. Intratumoral injection of
 526 thermogelling and sustained-release carboplatin-loaded hydrogel simplifies the
 527 administration and remains the synergistic effect with radiotherapy for mice gliomas.
 528 Biomaterials 2018;151:38-52.

529 [19] Liao C, Chen CS, Chen Y, Jiang N, Farn CJ, Shen Y, et al. Vancomycin-loaded
530 oxidized hyaluronic acid and adipic acid dihydrazide hydrogel: Bio-compatibility, drug
531 release, antimicrobial activity, and biofilm model. *Journal of Microbiology, Immunology*
532 *and Infection* 2019.

533 [20] Hernández-Montelongo J, Muñoz-Noval A, Torres-Costa V, Martín-Palma RJ, Manso-
534 Silvan M. Cyclic calcium phosphate electrodeposition on porous silicon.
535 *Int.J.Electrochem.Sci* 2012;7:1840-51.

536 [21] Martin-Palma RJ, Hernandez-Montelongo J, Torres-Costa V, Manso-Silvan M,
537 Munoz-Noval A. Nanostructured porous silicon-mediated drug delivery. *Expert opinion on*
538 *drug delivery* 2014;11(8):1273-83.

539 [22] Loya-Castro MF, Sánchez-Mejía M, Sánchez-Ramírez DR, Domínguez-Ríos R,
540 Escareño N, Ocegüera-Basurto PE, et al. Preparation of PLGA/Rose Bengal colloidal
541 particles by double emulsion and layer-by-layer for breast cancer treatment. *J.Colloid*
542 *Interface Sci.* 2018;518:122-9.

543 [23] Simmons H, Kontopoulou M. Hydrolytic degradation of branched PLA produced by
544 reactive extrusion. *Polym.Degrad.Stab.* 2018;158:228-37.

545 [24] Hernandez-Montelongo J, Lucchesi EG, Nascimento VF, Franca CG, Gonzalez I,
546 Macedo W, et al. Antibacterial and non-cytotoxic ultra-thin polyethylenimine film.
547 *Materials Science and Engineering: C* 2017;71:718-24.

548 [25] Hernández- Montelongo J, Oria L, Cárdenas AB, Benito N, Romero- Sáez M,
549 Recio- Sánchez G. Nanoporous silicon composite as potential system for sustained
550 delivery of florfenicol drug. *physica status solidi (b)* 2018;255(10):1700626.

551 [26] Mosmann T. Rapid colorimetric assay for cellular growth and survival: application to
552 proliferation and cytotoxicity assays. *J.Immunol.Methods* 1983;65(1-2):55-63.

553 [27] Guzmán-Oyarzo D, Plaza T, Recio-Sánchez G, Abdalla DS, Salazar LA, Hernández-
554 Montelongo J. Use of nPSi-βCD Composite Microparticles for the Controlled Release of
555 Caffeic Acid and Pinocembrin, Two Main Polyphenolic Compounds Found in a Chilean
556 Propolis. *Pharmaceutics* 2019;11(6):289.

557 [28] Sun D, Kang S, Liu C, Lu Q, Cui L, Hu B. Effect of zeta potential and particle size on
558 the stability of SiO₂ nanospheres as carrier for ultrasound imaging contrast agents.
559 *Int.J.Electrochem.Sci* 2016;11(10):8520-9.

560 [29] Naveas N, Costa VT, Gallach D, Hernandez-Montelongo J, Palma RJM, Garcia-Ruiz
561 JP, et al. Chemical stabilization of porous silicon for enhanced biofunctionalization with
562 immunoglobulin. *Science and technology of advanced materials* 2012;13(4):045009.

- [30] Tolstoy VP, Chernyshova I, Skryshevsky VA. Handbook of infrared spectroscopy of ultrathin films. : John Wiley & Sons; 2003.
- [31] Mawhinney DB, Glass JA, Yates JT. FTIR study of the oxidation of porous silicon. The Journal of Physical Chemistry B 1997;101(7):1202-6.
- [32] Kharin AY, Kargina YV, Timoshenko VY. Evolution of nanocrystal size distribution in porous silicon nanoparticles during storage in aqueous media: X-ray diffraction analysis. Journal of Nanoparticle Research 2019;21(2):27.
- [33] Siepmann J, Siepmann F. Mathematical modeling of drug delivery. Int.J.Pharm. 2008;364(2):328-43.
- [34] Hernandez-Montelongo J, Naveas N, Degoutin S, Tabary N, Chai F, Spampinato V, et al. Porous silicon-cyclodextrin based polymer composites for drug delivery applications. Carbohydr.Polym. 2014;110:238-52.
- [35] Li N, Fu C, Zhang L. Using casein and oxidized hyaluronic acid to form biocompatible composite hydrogels for controlled drug release. Materials Science and Engineering: C 2014;36:287-93.

Figure captions

Table 1. *In-vitro* release kinetics of Rose Bengal in PBS at 37 °C.

Figure 1. A) SEM image of nPSi microparticles. B) Particle size distribution.

Figure 2. Chemical structure of oxi-HA/ADH hydrogel.

Figure 3. Optical microscopy images of hydrogels: A) oxi-HA/ADH, B) oxi-HA/ADH with 0.1% nPSi, C) oxi-HA/ADH with 0.5%, and D) oxi-HA/ADH 1.0%. Insets are representative images of each sample ($\varnothing \approx 9$ mm, $h \approx 4$ mm). SEM images of hydrogels: E) oxi-HA/ADH, F) oxi-HA/ADH with 0.1% nPSi, G) oxi-HA/ADH with 0.5% nPSi, and H) oxi-HA/ADH with 1.0% nPSi.

Figure 4. A) UV-Vis spectra of hydrogels, B) FTIR-ATR spectra of hydrogels, and C) XRD analysis of hydrogels.

Figure 5. Mechanical properties of the hydrogels: A) Compressive force, and B) Stress strength. C) Residual mass as a function of hydrolysis time (PBS medium at pH 7.4 and 37 °C).

Figure 6. RB release profiles: A) nPSi microparticles, B) pure oxi-HA/ADH hydrogel with different RB%, and C) oxi-HA/ADH hydrogel with different nPSi%, which was previously loaded with RB.

Figure 7. Korsmeyer-Peppas model fitting of RB release profiles: A) nPSi microparticles, B) pure oxi-HA/ADH hydrogel with different RB%, and C) oxi-HA/ADH hydrogel with different nPSi%, which was previously loaded with RB.

Figure 8. A) Cytotoxicity of nPSi microparticles. B) Cell viability of hydrogels.

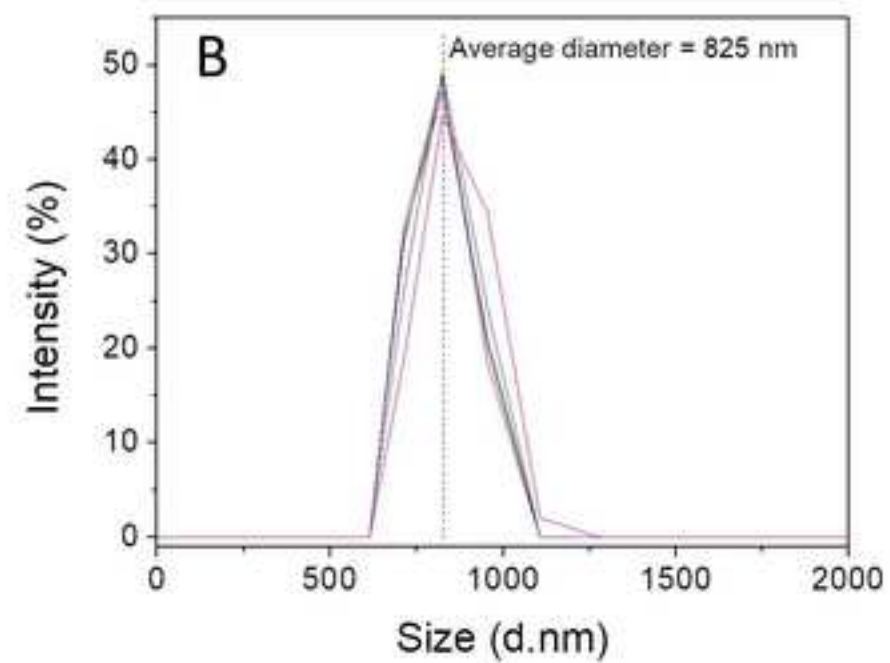
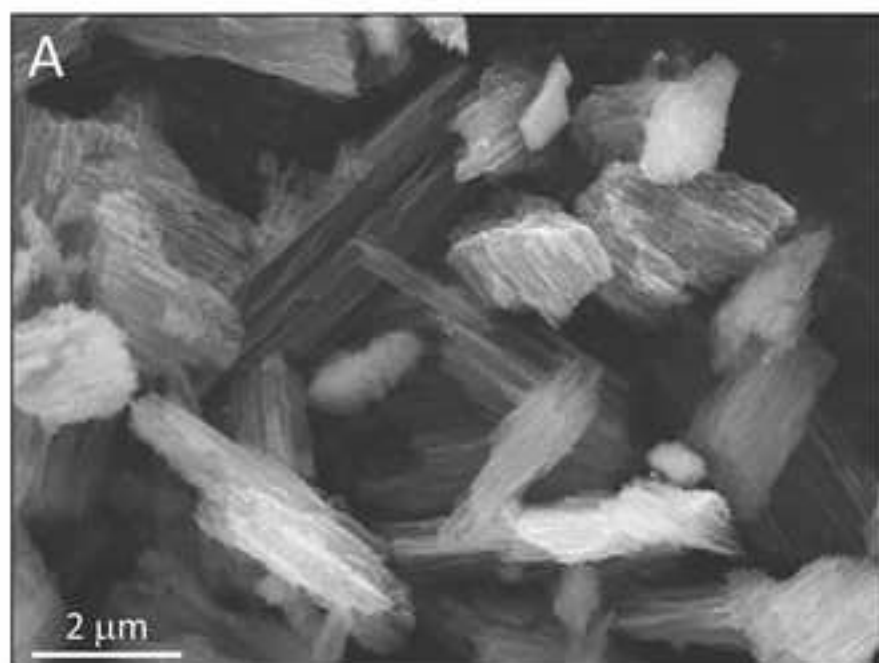


Figure 2

[Click here to access/download;Figure\(s\);Fig 2.jpg](#)

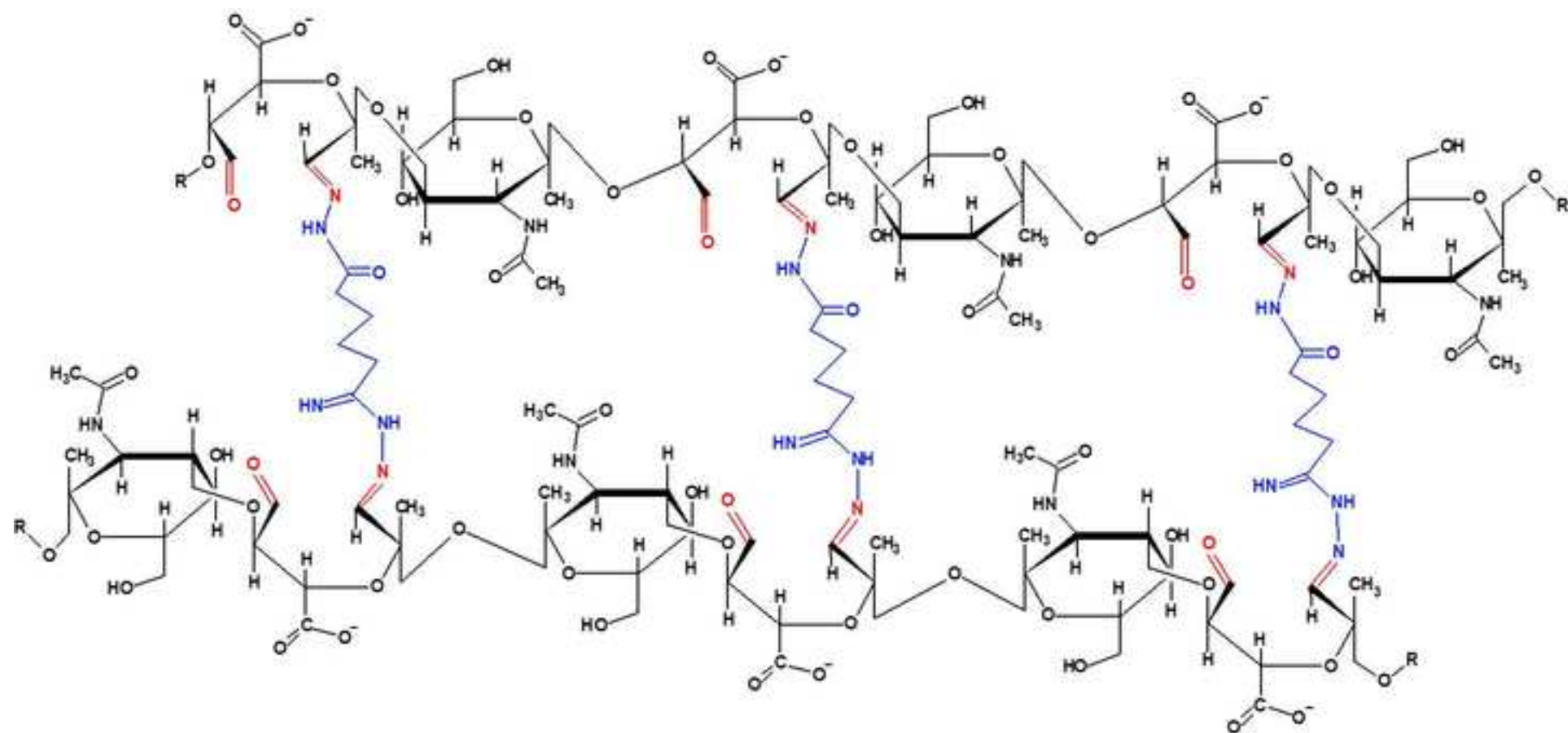
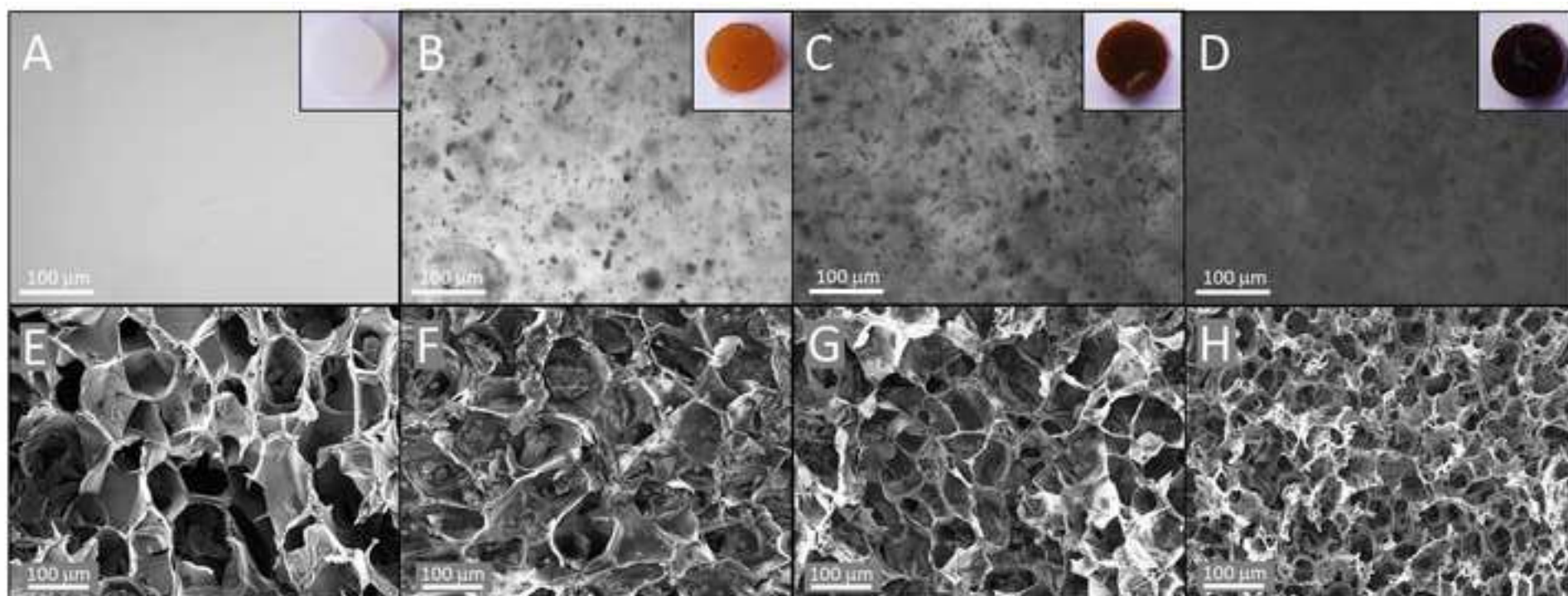
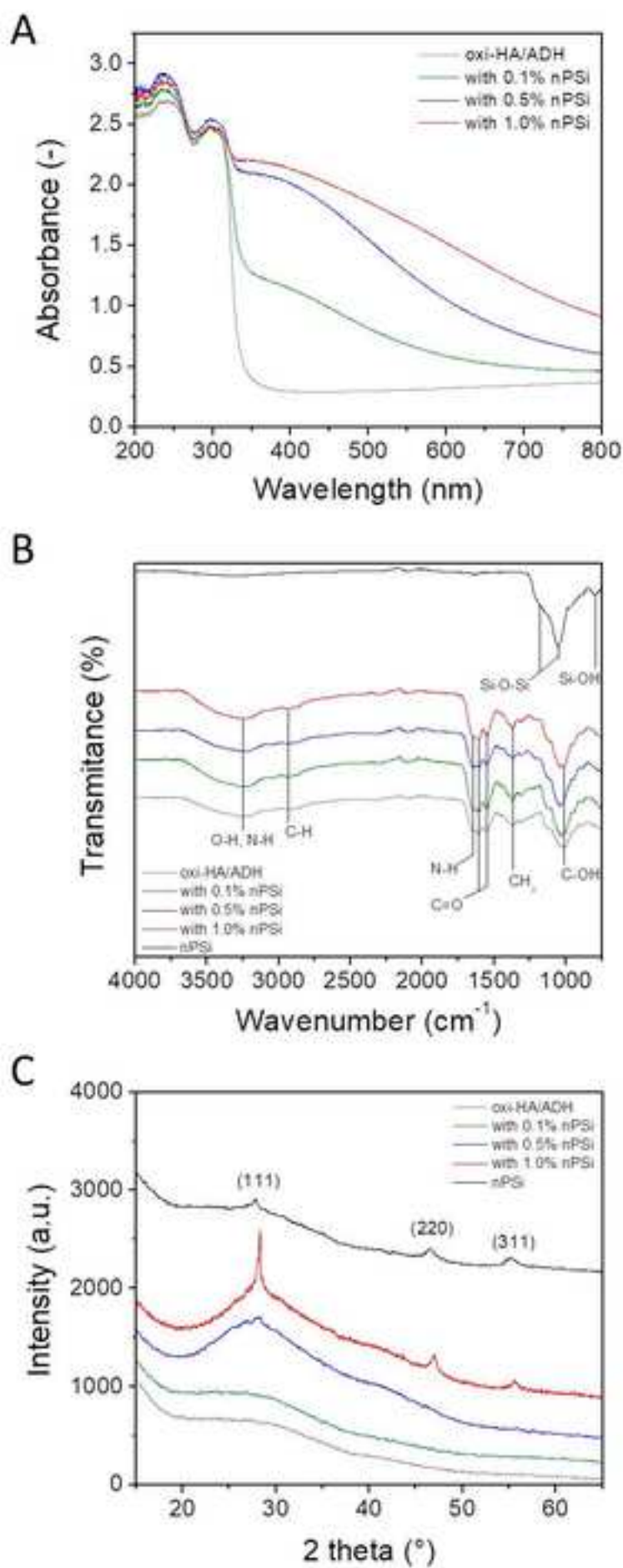
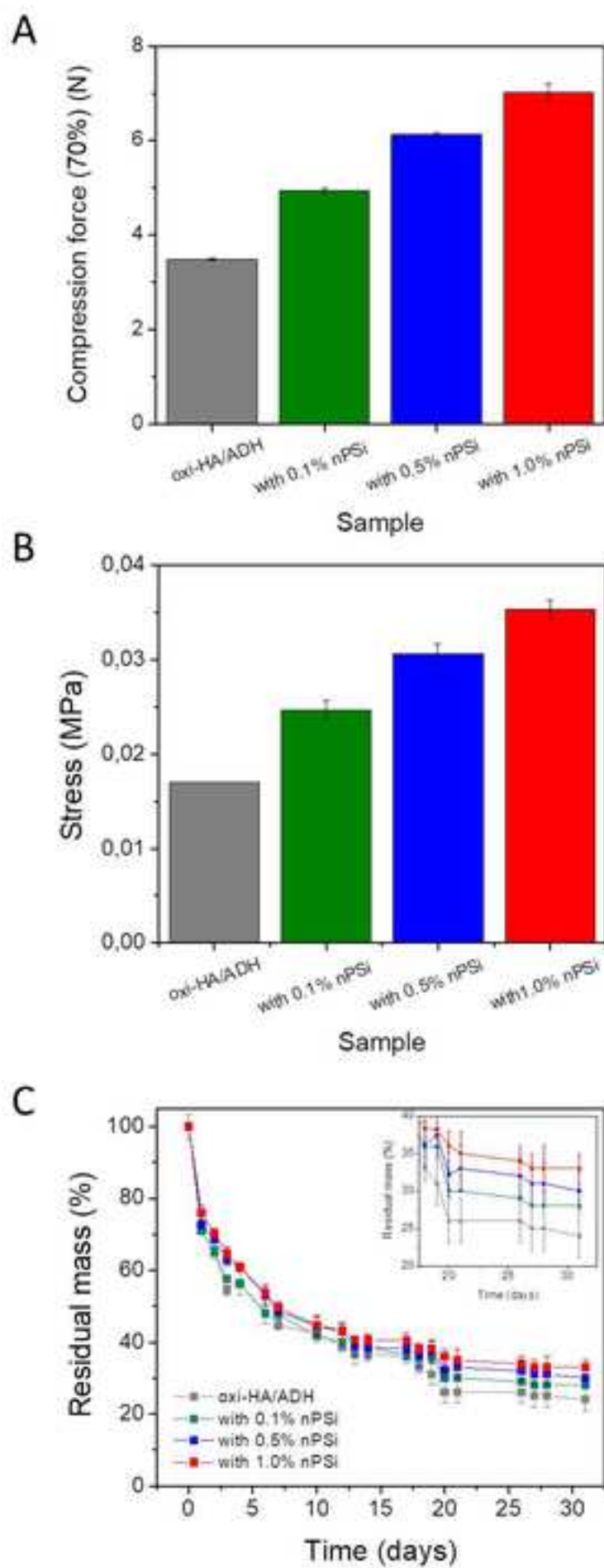


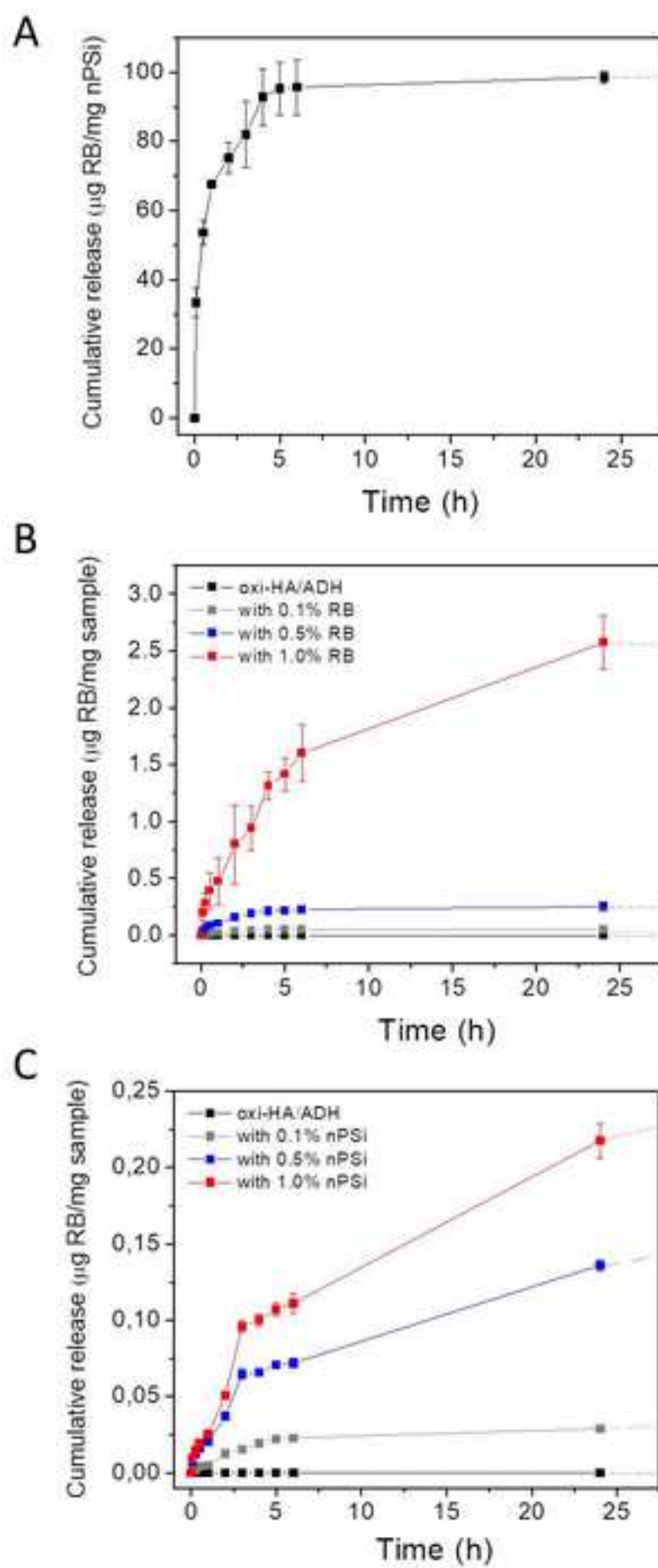
Figure 3

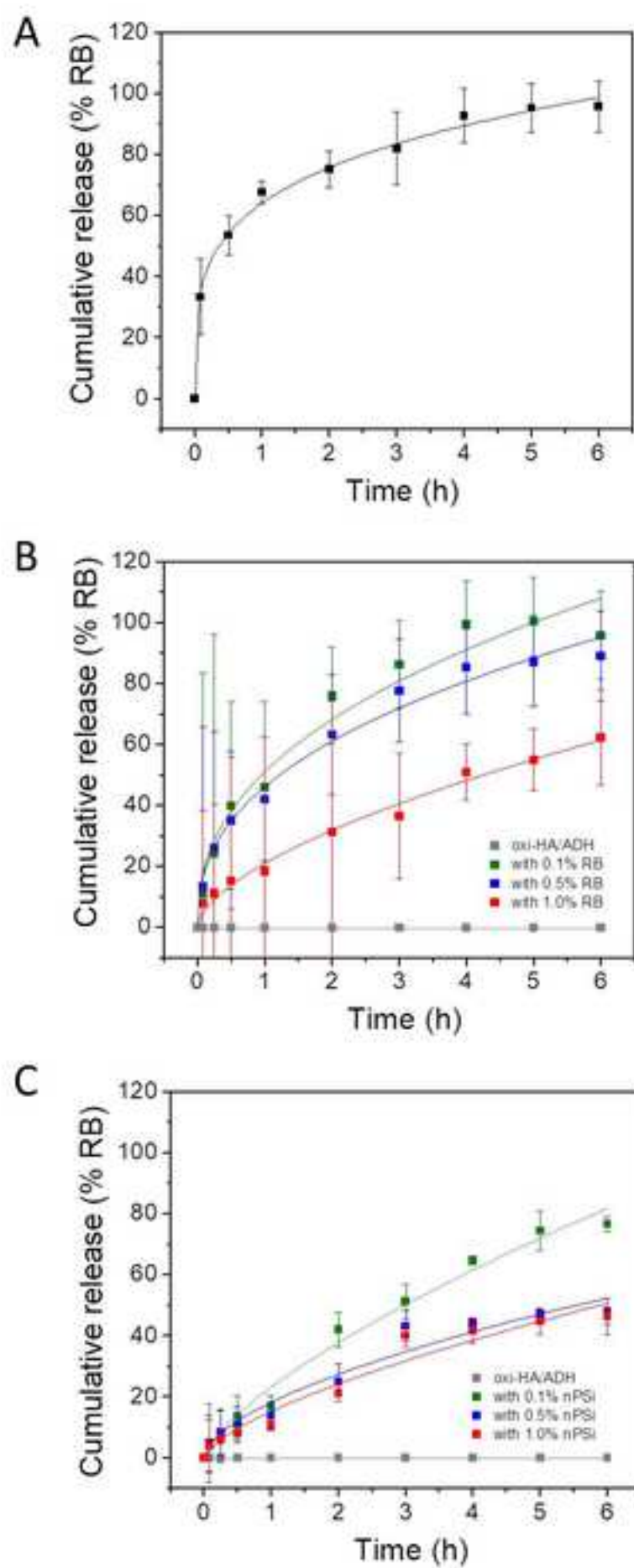
[Click here to access/download;Figure\(s\);Fig 3.jpg](#)











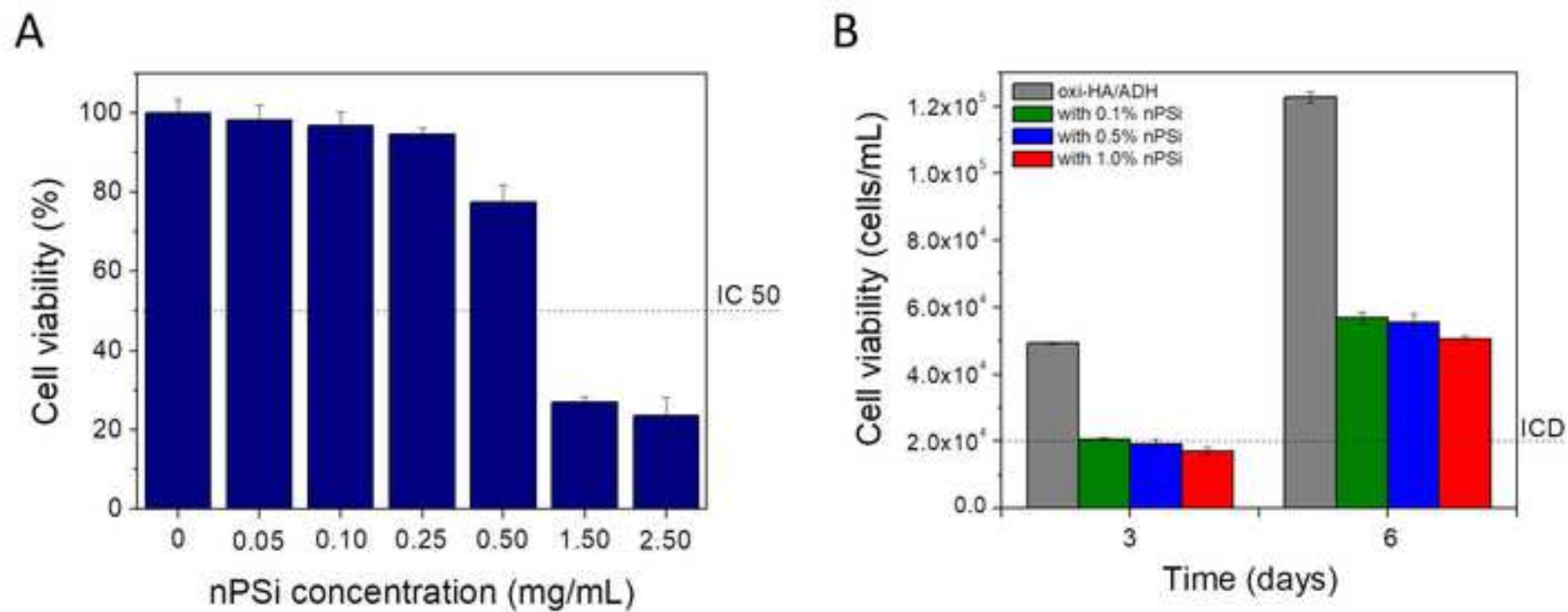


Table 1. *In-vitro* release kinetics of Rose Bengal in PBS at 37 °C.

Sample	RB in sample initially (µg/mg)	RB released from initial load (%)	RB released (µg/mg)	Korsmeyer-Peppas model		
				$\frac{M_t}{M_\infty} = k_{KP} t^n$		
				$k_{KP}(h^{-n})$	n	r_{adj}^2
nPSi	101.0±3.0	98.0±1 at 24 h	99±1 at 24 h	64.1723	0.2405	0.9946
oxi-HA/ADH	-	-	-	-	-	-
with 0.1% RB	1.67±0.13	3.33±0.54 at 24 h	0.055±0.001 at 24 h	51.002	0.4186	0.9658
with 0.5% RB	8.17±0.52	3.33±0.47 at 24 h	0.255±0.040 at 24 h	46.1206	0.4042	0.9855
with 1.0% RB	15.98±2.09	16.2±1.60 at 24 h	2.55±0.25 at 24 h	20.9826	0.5997	0.9876
with 0.1% nPSi	0.168±0.001	17.9±1.5 at 72 h	0.030±0.002 at 72 h	23.2571	0.7018	0.9853
with 0.5% nPSi	0.905±0.030	16.6±1.0 at 72 h	0.150±0.007 at 72 h	18.2185	0.5907	0.9585
with 1.0% nPSi	1.720±0.054	14.5±1.0 at 72 h	0.250±0.014 at 72 h	15.2761	0.6687	0.9541

Authors contributions

CGF and JHM conceived and designed experiments; TP and GR synthesized the nPSi microparticles; CGF and TP synthesized hydrogels and hydrogels with microparticles; NN and MMS performed the microscopy characterization; CGF and TP performed the physicochemical characterization and mechanical resistance tests; CGF and MHAS performed the biological experiments; CGF and JHM analyzed the data; MHAS, MMS and JHM contributed reagents/materials/analysis tools; CGF and JHM wrote the manuscript. All authors revised the manuscript.

Declaration of interests

☒ The authors declare that they have no known competing financial interests or personal relationships that could have appeared to influence the work reported in this paper.

☐ The authors declare the following financial interests/personal relationships which may be considered as potential competing interests:

Carla Giometti França, Tanya Plaza, Nelson Naveas, Maria Helena Andrade Santana, Miguel Manso-Silván, Gonzalo Recio, Jacobo Hernandez-Montelongo (corresponding author).

